

## Collective Oscillations of an Imbalanced Fermi Gas: Axial Compression Modes and Polaron Effective Mass

S. Nascimbène, N. Navon, K. J. Jiang, L. Tarruell,\* M. Teichmann,† J. McKeever,‡ F. Chevy, and C. Salomon

Laboratoire Kastler Brossel, CNRS, UPMC, École Normale Supérieure, 24 rue Lhomond, 75231 Paris, France

(Received 15 July 2009; revised manuscript received 2 October 2009; published 20 October 2009)

We investigate the low-lying compression modes of a unitary Fermi gas with imbalanced spin populations. For low polarization, the strong coupling between the two spin components leads to a hydrodynamic behavior of the cloud. For large population imbalance we observe a decoupling of the oscillations of the two spin components, giving access to the effective mass of the Fermi polaron, a quasiparticle composed of an impurity dressed by particle-hole pair excitations in a surrounding Fermi sea. We find  $m^*/m = 1.17(10)$ , in agreement with the most recent theoretical predictions.

DOI: 10.1103/PhysRevLett.103.170402

PACS numbers: 03.75.Ss, 05.30.Fk, 32.30.Bv, 67.60.Fp

The study of the low-lying excitation modes of a complex system can be a powerful tool for investigation of its physical properties. For instance, Earth's structure has been probed using the propagation of seismic waves in the mantle, and the ripples in space-time propagated by gravitational waves can be used as probes of extreme cosmic phenomena. In ultracold atomic gases, the measurement of low energy modes of bosonic or fermionic systems has been used to probe superfluidity effects [1], to measure the angular momentum of vortex lattices [2], and to characterize the equation of state of fermionic superfluids [3,4].

In this Letter, we study the excitation spectrum of an ultracold Fermi gas with imbalanced spin populations. This topic was initiated in the 1960s by the seminal works of Clogston and Chandrasekhar [5,6] and only recently found experimental confirmation thanks to the latest developments in ultracold Fermi gases [7,8]. These dramatic experiments have observed that when a fermionic superfluid is polarized through imbalance of spin populations, the trapped atomic cloud forms a shell structure. The energy gap associated with pairing maintains a superfluid core where the two spin densities are equal, while the outer shell is composed by a normal gas with imbalanced spin densities (see Fig. 1). Here, we extend this work to the unexplored dynamical properties of these systems and we focus on the regime of strong interactions, where the scattering length  $a$  is infinite. We show, in particular, that the study of the axial breathing mode provides valuable insight on the dynamical properties of a quasiparticle, the Fermi polaron, that was introduced recently to describe the normal component occupying the outer shell of the cloud [9–14]. The Fermi polaron is composed of an impurity (labeled 2) immersed in a noninteracting Fermi sea (labeled 1), and is analogous to the polaron of condensed matter physics, i.e., an electron immersed in a bath of noninteracting (bosonic) phonons. Understanding the static and dynamic properties of impurities immersed in an external bath is a paradigm of many-body systems. In addition

to polaron physics, famous examples include the Kondo effect, Higgs mechanism, or the dressed atom. Despite its apparent simplicity, this problem remains today very challenging in the limit of strong interactions.

According to the Landau theory of the Fermi liquid, the low energy spectrum of the polaron is similar to that of a free particle and can, in the local density approximation (LDA), be recast as

$$E_2(\mathbf{r}, \mathbf{p}) = AE_{F1}(\mathbf{r}) + V(\mathbf{r}) + \frac{p^2}{2m^*} + \dots \quad (1)$$

where  $V$  is the trapping potential,  $E_{F1}(\mathbf{r}) = E_{F1}(0) - V(\mathbf{r})$

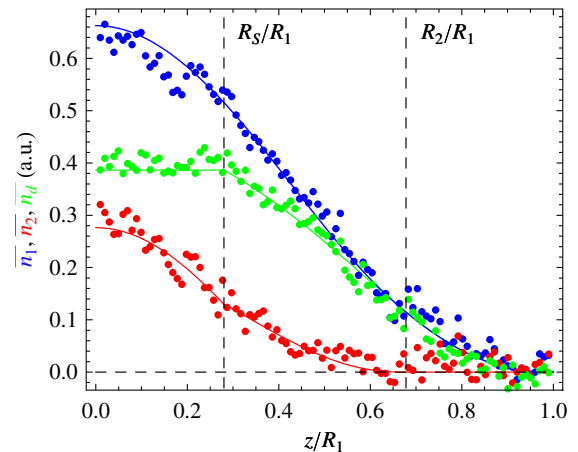


FIG. 1 (color online). Integrated density profiles of an imbalanced Fermi gas. Blue (dark gray): majority atoms  $\bar{n}_1(z)$ ; Red (medium gray): minority atoms  $\bar{n}_2(z)$ ; Green (light gray): difference  $\bar{n}_d = \bar{n}_1 - \bar{n}_2$ . In this latter case, the flat-top feature signals a cancellation of the density difference at the center of the trap, characteristic of the existence of a fully paired superfluid core. The superfluid (resp. minority) radius  $R_S$  (resp.  $R_2$ ) are marked by vertical dashed lines. The solid color lines correspond to the prediction of Monte Carlo theories [20], the only fit parameters being the number of atoms in each spin state,  $N_1 = 8.0 \times 10^4$ ,  $N_2 = 2.4 \times 10^4$  for this image. The axial (radial) trap frequency is 18.6 Hz (420 Hz).

is the local Fermi energy of the majority species,  $A$  is a dimensionless quantity characterizing the attraction of the impurity by the majority atoms, and  $m^*$  is the effective mass of the Fermi polaron. For  $a = \infty$ ,  $A = -0.61$  has been determined both experimentally [14] and theoretically [9–13], while slight disagreements still exist on the value of the effective mass. Fixed node Monte Carlo suggests  $m^*/m = 1.09(2)$  [15], systematic diagrammatic expansion yields  $m^*/m = 1.20$  [11], and analysis of density profiles (such as Fig. 1) gives  $m^*/m = 1.06$  [16].

From Eq. (1), the quasiparticle evolves in an effective potential  $V^*(\mathbf{r}) = (1 - A)V(\mathbf{r})$ . Assuming  $V(\mathbf{r})$  to be harmonic with frequency  $\omega$ , the polaron is trapped in an effective potential of frequency  $\omega^*$  [9]:

$$\frac{\omega^*}{\omega} = \sqrt{\frac{1 - A}{m^*/m}}. \quad (2)$$

In this Letter we explore the compression mode properties and determine the effective mass through the measurement of the oscillation frequency  $\omega^*$  in the axial direction (labeled  $z$ ) of a cylindrically symmetric trap.

Our experimental setup is an upgraded version of the one presented in [17].  $7 \times 10^6$   ${}^6\text{Li}$  atoms in the hyperfine state  $|F = 3/2, m_F = +3/2\rangle$  are loaded into a mixed magnetic or optical trap at 100  $\mu\text{K}$ . The optical trap uses a single beam of waist  $w_0 = 35 \mu\text{m}$  and maximum power  $P = 60 \text{ W}$  operating at a wavelength  $\lambda = 1073 \text{ nm}$ . The atoms are transferred into the hyperfine ground state  $|1/2, 1/2\rangle$ , and a spin mixture is created by a radio-frequency sweep across the hyperfine transition  $|1/2, 1/2\rangle \rightarrow |1/2, -1/2\rangle$ . By varying the rate of this sweep, we control the sample's degree of polarization  $P \equiv (N_1 - N_2)/(N_1 + N_2)$ , where  $N_1$  (resp.  $N_2$ ) is the atom number of the majority (resp. minority) spin species. The mixture is then evaporatively cooled in 6 s by reducing the laser power to 70 mW. This is done at a magnetic field  $B = 834 \text{ G}$ , which corresponds to the position of the broad Feshbach resonance in  ${}^6\text{Li}$  where the scattering length is infinite and where further experiments are performed. Typical radial frequencies are  $\omega_x = \omega_y \sim 2\pi \times 400 \text{ Hz}$ . The axial confinement of the dipole trap is enhanced by the addition of a magnetic curvature, leading to an axial frequency  $\omega_z \sim 2\pi \times 30 \text{ Hz}$ . Our samples contain  $\sim 8 \times 10^4$  atoms in the majority spin state at a temperature  $T \lesssim 0.09T_F$ . The temperature is evaluated by fitting the wings of the majority density profile outside the minority radius. In this region, the gas is noninteracting, allowing unambiguous thermometry of the inner, strongly interacting part of the cloud [18]. Here,  $T_F$  is defined as the Fermi temperature of an ideal gas whose density profile overlaps the majority one in the fully polarized rim.

The two spin states are imaged sequentially using *in situ* absorption imaging. To prevent heating from the scattered photons and the strong interactions between the two species, the duration of the two imaging pulses as well as their separation must be short (10  $\mu\text{s}$  each). By reversing the

order in which we image the two spin components, we checked that imaging of the first species did not significantly influence the second. Typical integrated density profiles of the atom cloud  $\bar{n}(z) = \int dx dy n(x, y, z)$ , where  $n(x, y, z)$  is the 3D atom density, are presented in Fig. 1. These profiles display the characteristic features already observed by the MIT group [18]: a flat-top structure in the superfluid region confirming the existence of a fully paired core satisfying the LDA [19], an intermediate phase where the two spin species are present with unequal densities, and an outer rim containing only majority atoms. Following [20], we compare our density profiles to the prediction for the equation of state of the different phases and find fairly good agreement. In particular, we observe that the superfluid core disappears for polarizations  $P > 0.76(3)$ . This limit agrees well with the measurement of the MIT group [7] but differs from the Rice group value [8]. Our data also show no evidence for surface tension effects [8,21].

We excite the axial breathing mode by switching off the axial magnetic trapping field for 1 ms. The effect of this excitation is twofold: in addition to nearly suppressing the axial confinement, the bias field is increased up to 1050 G, where  $k_F a \sim -1$ , so that the gas is no longer strongly interacting. This scheme provides a spatially selective excitation of the cloud. Indeed, while the reduction of the trapping frequency perturbs the whole cloud, the modification of the scattering length only acts in the region where the two spin components overlap. In the regime of strong polarization, these two regions are well separated, leading to a differential excitation of the two spin components.

Let us first focus on the oscillations of the majority spin species presented in Fig. 2. Typical dynamics of the outer radius  $R_1(t)$  of the majority component are exemplified by Fig. 2(a). For each polarization, this time evolution is fitted using an exponentially damped sinusoid, with  $R_1(t) = R_1^{(0)}[1 + A_1 \cos(\omega_1 t + \varphi)]e^{-\gamma_1 t}$ , and the variations of  $\omega_1$  and  $\gamma_1$  as a function of  $P$  are displayed in Figs. 2(b) and 2(c). One remarkable feature of this graph is the frequency plateau for polarizations  $P \lesssim 0.7$ , corresponding approximately to the domain where a superfluid core is present in the cloud. Although in this range of parameters, the dynamics of the system is fairly complex due to the strong coupling between the superfluid and normal components, a simple argument based on a sum rule approach generalizing the result of [22] allows us to understand this property.

We describe the system by the Hamiltonian  $H = \sum_i p_i^2/2m + U(\mathbf{r}_1, \mathbf{r}_2, \dots)$ , where  $\mathbf{r}_i$  (resp.  $\mathbf{p}_i$ ) is the position (resp. momentum of particle  $i$ ),  $m$  is the mass of the atoms and  $U$  includes both trapping potential and interatomic interaction. The compression of the trapping frequency in the  $z$  direction is associated with the operator  $F = \sum_i z_i^2$ . Let us introduce the moments of the spectral distribution associated with  $F$  and defined by

$$m_k = \sum_{n \neq 0} (E_n - E_0)^k |\langle 0|F|n\rangle|^2,$$

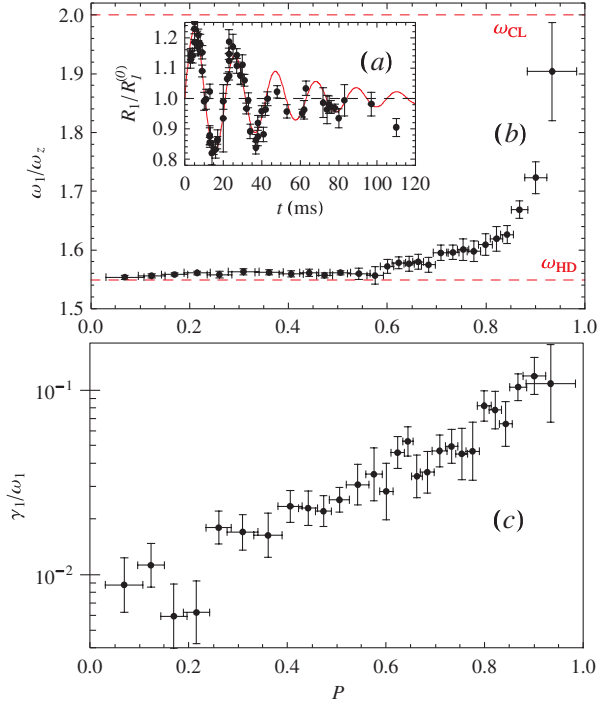


FIG. 2 (color online). (a) Oscillations of the axial radius of the majority component, for a population imbalance  $P = 0.85(2)$ , beyond the Clogston limit. The solid line corresponds to a fit by an exponentially damped sinusoid. (b) Frequency of the breathing mode  $\omega_1$  normalized to the axial trapping frequency  $\omega_z$  versus polarization. The superfluid (resp. collisionless) limits  $\omega_1 = \sqrt{12/5}\omega_z$  (resp.  $2\omega_z$ ) are indicated by the dashed red lines. The axial (radial) trap frequency is 28.9(1) Hz (420 Hz). (c) Damping rate  $\gamma_1$  versus polarization (in log scale). Note that our data are limited to  $P < 0.95$  due to the small minority atom number ( $N_2 \lesssim 2 \times 10^3$ ) at such high polarizations.

where the  $|n\rangle$  are the eigenstates of  $H$  associated with the eigenvalue  $E_n$ , and  $|0\rangle$  is the many-body ground state. We assume that the operator  $F$  mainly couples  $|0\rangle$  to one excited state  $|1\rangle$ . In this case, the frequency of the breathing mode excited by the axial compression of the trap is given by  $\omega_1 = (E_1 - E_0)/\hbar \simeq \sqrt{m_1/m_{-1}}/\hbar$ . An explicit calculation of these two moments leads to the following expression:

$$\omega_1^2 \simeq -2\langle z^2 \rangle / \frac{\partial \langle z^2 \rangle}{\partial \omega_z^2}. \quad (3)$$

For a unitary gas, LDA imposes that the mean radius of the cloud is given by  $\langle z^2 \rangle = R_{TF}^2 f(P)$ , where  $R_{TF}$  is the radius of an ideal Fermi gas in the same trap and with the same atom number and  $f$  is some universal function of the polarization [23]. Using this assumption, the calculation of the oscillation frequency is straightforward and yields  $\sqrt{12/5}\omega_z = 1.55\omega_z$ , i.e., the hydrodynamic prediction [3,24] for  $P = 0$ , regardless of the polarization of the sample. This argument is in good agreement with our experimental findings [Fig. 2(b)].

At larger polarizations the frequency sharply increases towards the collisionless value. The damping rate, very small in the balanced superfluid, increases by a factor  $\sim 20$  for higher imbalances [25]. Interestingly, as seen in Fig. 3, this behavior is consistent with a general argument about relaxation processes in fluid dynamics [26]. Indeed, one can relate  $\omega_1$  and  $\gamma_1$  through

$$\omega^2 = \omega_{CL}^2 + \frac{\omega_{HD}^2 - \omega_{CL}^2}{1 + i\omega\tau}, \quad (4)$$

where  $\omega = \omega_1 + i\gamma_1$ ,  $\omega_{HD} = \sqrt{12/5}\omega_z$  (resp.  $\omega_{CL} = 2\omega_z$ ) is the hydrodynamic (resp. collisionless) frequency and  $\tau$  is an effective relaxation rate.

Measurements of  $\omega_1/\omega_z$  in three different traps of aspect ratios 8.2, 9.0, and 14.5 give identical results (within 3%) for all polarizations. By contrast, the effect of temperature is more pronounced: for instance at  $0.12(1)T_F$ ,  $\omega_1(P)$  remains equal to the hydrodynamic prediction at all attainable polarizations with  $P_{max} = 0.95$ , for a cloud of  $N_1 \sim 2 \times 10^5$  majority atoms held in a trap of aspect ratio 22. This illustrates the role of Pauli blocking at the lowest temperatures which favors collisionless behavior. This is in contrast with the balanced gas case where the collisionless regime was observed at higher temperature ( $T \gtrsim T_F$ ) [27].

Let us now consider the dynamics of the minority cloud (we recall that subscript 2 refers to the impurity atoms). We observe that for polarizations smaller than  $P \sim 0.75$ , the oscillation frequencies and damping rates of the two spin species are equal, indicating a strong coupling between them. By contrast, for  $P > 0.75$ , a Fourier spectrum of  $R_2(t)$  reveals two frequencies [Fig. 4(a)], a generic feature of systems with multiple phases [28,29]. The lower frequency  $\omega_{2a}$  is equal to the majority oscillation frequency  $\omega_1$ . We interpret the higher frequency  $\omega_{2b}$ , whose weight increases with polarization, as the axial breathing of the minority atoms out of phase with the majority cloud. A linear extrapolation of this frequency to  $P = 1$  gives the oscillation frequency of a dilute gas of weakly interacting polarons inside a Fermi sea at rest,  $\omega_{2b}(P \rightarrow 1) = 2.35(10)\omega_z$  [Fig. 4(b)]. The uncertainty represents the standard deviation of a linear fit taking into account the

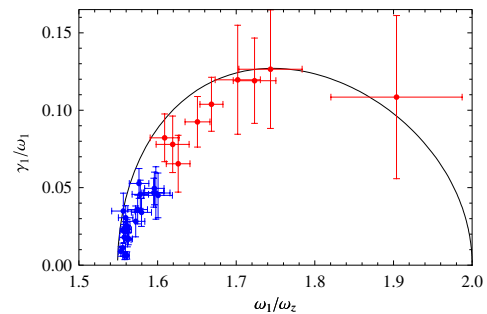


FIG. 3 (color online). Comparison of our experimental results with the parametric curve  $(\omega_1(\tau)/\omega_z, \gamma_1(\tau)/\omega_1(\tau))$  deduced from prediction (4). The data in blue (dark gray) [red (medium gray)] correspond to polarizations  $P < 0.8$  [ $P > 0.8$ ].

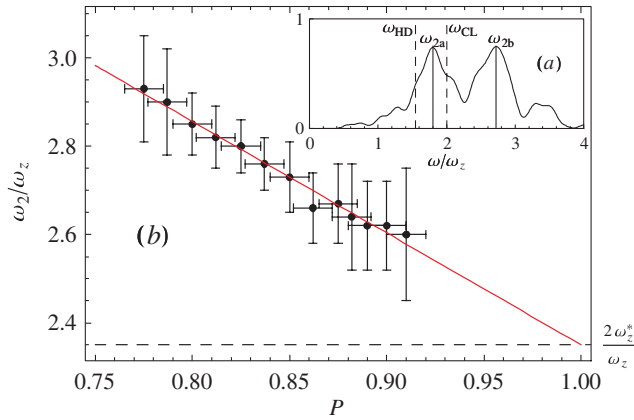


FIG. 4 (color online). (a) Frequency power spectrum of the minority spin state for  $P = 0.90(2)$ . The peak between  $\omega_{HD}$  and  $\omega_{CL}$  corresponds to the oscillation in phase with the majority, the other one to the polaron oscillation. (b) Frequency of the polaron component as a function of polarization. All frequencies are normalized to  $\omega_z$ .

statistical uncertainties of the  $\omega_{2b}$  measurements for each polarization.

By identifying the breathing mode frequency  $\omega_{2b}$  as  $2\omega_z^*$  and using (2), we deduce the mass of the quasiparticle:  $m^*/m = 1.17(10)$ . This is the first dynamic measurement of the polaron effective mass, in good agreement with the most recent theoretical predictions [11,15]. The previous measurement of  $m^*$  through analysis of density profiles required an approximate equation of state for the polaron gas, with uncontrolled accuracy [16]. Extrapolating  $\omega_{2b}(P)$  to  $P = 1$  allows us to overcome this issue.  $m^*$  is close to  $m$  (albeit different), a surprising feature for a system at unitarity.

In conclusion, we have studied the low frequency breathing modes of an elongated Fermi gas with imbalanced spin populations. In the presence of a superfluid core, the majority and minority components oscillate in phase with a frequency that is largely independent of the spin polarization. At strong polarizations, the minority atom oscillation reveals a second frequency, that we interpret as the Fermi polaron breathing mode. Further investigations will extend our work to all values of the scattering length. In particular, they should provide a clear signature of the polaron-molecule transition [14,30]. The role of interactions between polarons and damping phenomena should also be clarified [31].

We are grateful to S. Stringari, A. Recati, C. Lobo, M. Zwierlein, J. Dalibard, and Y. Castin for fruitful discussions as well as K. Magalhães and G. Duffy for experimental support. We acknowledge support from ESF (FerMix), SCALA, ANR FABIOLA, Région Ile de France (IFRAF), ERC and Institut Universitaire de France.

\*Present address: Institute for Quantum Electronics, ETH Zurich, 8093 Zurich, Switzerland.

†Present address: Max-Born-Institut, Max-Born-Strasse 2 A, 12489 Berlin, Germany.

‡Present address: IOS, CQIQC and Department of Physics, University of Toronto, Canada.

- [1] S. Giorgini, L. Pitaevskii, and S. Stringari, *Rev. Mod. Phys.* **80**, 1215 (2008).
- [2] F. Chevy, K. W. Madison, and J. Dalibard, *Phys. Rev. Lett.* **85**, 2223 (2000).
- [3] M. Bartenstein, A. Altmeyer, S. Riedl, S. Jochim, C. Chin, J. Denschlag, and R. Grimm, *Phys. Rev. Lett.* **92**, 203201 (2004).
- [4] J. Kinast, S. Hemmer, M. Gehm, A. Turlapov, and J. Thomas, *Phys. Rev. Lett.* **92**, 150402 (2004).
- [5] A. Clogston, *Phys. Rev. Lett.* **9**, 266 (1962).
- [6] B. S. Chandrasekhar, *Appl. Phys. Lett.* **1**, 7 (1962).
- [7] M. Zwierlein, A. Schirotzek, C. Schunck, and W. Ketterle, *Science* **311**, 492 (2006).
- [8] G. Partridge, W. Li, R. Kamar, Y. Liao, and R. Hulet, *Science* **311**, 503 (2006).
- [9] C. Lobo, A. Recati, S. Giorgini, and S. Stringari, *Phys. Rev. Lett.* **97**, 200403 (2006).
- [10] F. Chevy, *Phys. Rev. A* **74**, 063628 (2006).
- [11] R. Combescot and S. Giraud, *Phys. Rev. Lett.* **101**, 050404 (2008).
- [12] R. Combescot, A. Recati, C. Lobo, and F. Chevy, *Phys. Rev. Lett.* **98**, 180402 (2007).
- [13] N. Prokof'ev and B. Svistunov, *Phys. Rev. B* **77**, 125101 (2008).
- [14] A. Schirotzek, C.-H. Wu, A. Sommer, and M. W. Zwierlein, *Phys. Rev. Lett.* **102**, 230402 (2009).
- [15] S. Pilati and S. Giorgini, *Phys. Rev. Lett.* **100**, 030401 (2008).
- [16] Y. Shin, *Phys. Rev. A* **77**, 041603 (2008).
- [17] T. Bourdel, L. Khaykovich, J. Cubizolles, J. Zhang, F. Chevy, M. Teichmann, L. Tarruell, S. Kokkelmans, and C. Salomon, *Phys. Rev. Lett.* **93**, 050401 (2004).
- [18] Y. Shin, C. Schunck, A. Schirotzek, and W. Ketterle, *Nature (London)* **451**, 689 (2008).
- [19] M. Haque and H. Stoof, *Phys. Rev. A* **74**, 011602 (2006).
- [20] A. Recati, C. Lobo, and S. Stringari, *Phys. Rev. A* **78**, 023633 (2008).
- [21] T. De Silva and E. Mueller, *Phys. Rev. Lett.* **97**, 070402 (2006).
- [22] L. Vichi and S. Stringari, *Phys. Rev. A* **60**, 4734 (1999).
- [23] F. Chevy, *Phys. Rev. Lett.* **96**, 130401 (2006).
- [24] M. Amoruso, I. Meccoli, A. Minguzzi, and M. Tosi, *Eur. Phys. J. D* **7**, 441 (1999).
- [25] The damping rate is expected to vanish in the truly collisionless limit, a regime difficult to access experimentally.
- [26] L. Landau and E. Lifshitz, *Fluid Mechanics*, Course of Theoretical Physics Vol. 6 (Butterworth-Heinemann, Oxford, 1987).
- [27] S. Riedl, E. Sánchez Guajardo, C. Kohstall, A. Altmeyer, M. Wright, J. Denschlag, R. Grimm, G. Bruun, and H. Smith, *Phys. Rev. A* **78**, 053609 (2008).
- [28] M. Urban, *Phys. Rev. A* **78**, 053619 (2008).
- [29] G. Bruun and B. Mottelson, *Phys. Rev. Lett.* **87**, 270403 (2001).
- [30] N. Prokof'ev and B. Svistunov, *Phys. Rev. B* **77**, 020408 (2008).
- [31] G. Bruun, A. Recati, C. Pethick, H. Smith, and S. Stringari, *Phys. Rev. Lett.* **100**, 240406 (2008).